Fréchet kernels based on a fractional viscoacoustic wave equation

Guangchi Xing and Tieyuan Zhu, Department of Geosciences, The Pennsylvania State University

SUMMARY

Incorporating the seismic attenuation into the waveform inversion framework could not only improve the accuracy of the velocity model but also provide an additional Q model. Recently, we proposed a viscoacoustic wave equation assisted by the fractional Laplacian operators to accurately model the wave propagation in heterogeneous attenuating media with computational efficiency. The explicit presence of Q as a coefficient in this equation suggests the potential to conveniently develop its full waveform inversion scheme. In this study, we utilize the adjoint-state method to formulate the computation of the Fréchet kernels with respect to both velocity and attenuation based on this wave equation. These kernels will play a fundamental role in the viscoacoustic multiparameter waveform inversion.

INTRODUCTION

Full waveform inversion (FWI, e.g. Virieux and Operto 2009) as well as the more general adjoint tomography (e.g. Tromp et al. 2005) utilizes the adjoint-state method (e.g. Plessix 2006) to minimize the residual between observed and synthetic seismograms by iteratively adjusting the model parameters. In this process, the Fréchet kernel (the gradient of the objective function with respect to the model parameters) is computed by interacting the forward and the adjoint wavefields at each iteration to refine the initial model into a high-resolution final model. The quality of the final model critically depends on whether the forward and the adjoint modelings take into account all the relevant wave physics (Tarantola, 1988). Seismic attenuation, quantified by the quality factor Q, has a significant impact on both the amplitude and phase of seismograms, especially in the presence of fluid in porous media (White, 1975; Dvorkin and Mavko, 2006; Müller et al., 2010). Thus, it is crucial to incorporate the viscoelasticity into the computation of the Fréchet kernel as we can not only enhance the accuracy and reliability of the resultant velocity model but can also obtain a Q model.

One popular method to model the attenuating wavefield in the time domain is superposing rheological bodies (e.g. Maxwell, Kelvin-Voigt, Zener) to approximate the constant-Q observations (McDonal et al., 1958; Knopoff, 1964) and introducing memory variables to solve the viscoacoustic/viscoelastic wave equation (Emmerich and Korn, 1987; Carcione et al., 1988; Robertsson et al., 1994). Based on this method, Bai et al. (2014) derive the adjoint-based theoretical framework for velocity inversion. The development of the attenuation inversion, however, is hindered by its implicit Q encoding. Fichtner and van Driel (2014) parametrize the attenuation mechanisms via a curve-fitting process to allow the explicit presence of Q in the wave equation and compute the corresponding Fréchet kernels. Yang et al. (2016) establish the systematic formulation for multiparameter viscoelastic FWI based on the memory variable method.

On the other hand, several studies propose wave equations assisted by the fractional Laplacian operators to model the viscoacoustic waves (e.g. Zhu and Harris 2014; Chen et al. 2016; Yang and Zhu 2018) and viscoelastic waves (Zhu and Carcione, 2013; Wang et al., 2017). These equations rigorously characterize the constant-Q property (Kjartansson, 1979) without the necessity to introduce the memory variables, and, uniquely, have separate controls over dissipation and dispersion effects. Taking advantage of it, Xue et al. (2017) conduct the Q-compensated FWI to accelerate the convergence. Recently, Xing and Zhu (2018) propose a viscoacoustic wave equation with fixed Fractional Laplacian powers that can accurately simulate the wavefield in heterogeneous Q media. Meanwhile, the Q appears explicitly as coefficients in this equation, which makes it straightforward to formulate the inverse problem.

In this study, we derive the formulations to compute the adjoint-state Fréchet kernels associated with this viscoacoustic wave equation. We first present the fractional wave equation based on the Kjartansson constant-Q model. On the top of it, we derive its adjoint operator and the Fréchet kernels for various objective functions. Finally, we conduct numerical experiments to implement the kernel computation algorithm.

FORWARD MODELING

The Kjartansson model represents a frequency-independent Q with only three parameters (Kjartansson, 1979): the reference angular frequency ω_0, its corresponding phase velocity c_0 and a Q-related dimensionless parameter $\gamma = \frac{1}{\pi} arctan(\frac{1}{Q})$. Based on this model, Xing and Zhu (2018) propose a viscoacoustic wave equation:

$$\mathbf{L}u = (\mathbf{L_0} + \mathbf{L_1} + \mathbf{L_2})u = f, \tag{1}$$

$$\mathbf{L_0} = \frac{1}{c^2}\frac{\partial^2}{\partial t^2} - \nabla^2, \tag{2}$$

$$\mathbf{L_1} = -\gamma\frac{\omega_0}{c}(-\nabla^2)^{\frac{1}{2}} + \gamma\frac{c}{\omega_0}(-\nabla^2)^{\frac{3}{2}}, \tag{3}$$

$$\mathbf{L_2} = (\pi\gamma\frac{1}{c}(-\nabla^2)^{\frac{1}{2}} - \pi\gamma^2\frac{1}{\omega_0}\nabla^2)\frac{\partial}{\partial t}, \tag{4}$$

where u is the pressure wavefield, f is the source term and $c = c_0 cos(\frac{\pi\gamma}{2})$ is a reference velocity. As shown in Equation (1), the wave propagation operator $\mathbf{L}$ has three contributions: $\mathbf{L_0}$ the lossless acoustic wave propagator,

10.1190/segam2019-3215198.1

$\mathbf{L_1}$ the phase dispersion corrector and $\mathbf{L_2}$ the amplitude loss corrector. This wave equation is implemented using the pseudospectral method to model the viscoacoustic wavefield accurately and efficiently.

FRÉCHET KERNELS

Following the Lagrangian multiplier method (Plessix, 2006), we can formulate the computation of Fréchet kernels K with Equation (1) for forward modeling as well as two extra equations for adjoint modeling and wavefield interaction, respectively:

$$\mathbf{L}^*\lambda = \frac{\partial J}{\partial u}, \tag{5}$$

$$K = \frac{dJ}{dm} = -\langle \lambda, \frac{\partial \mathbf{L}}{\partial m} u \rangle, \tag{6}$$

where $*$ denotes adjoint, λ is the adjoint wavefield, J is the objective function and m is the model parameter.

Objective functions

We consider three objective functions, i.e., the misfit of waveform, cross-correlation traveltime and amplitude. For different objective functions, the adjoint wavefields are excited by different adjoint sources as in Equation (5). The waveform objective function $J_W = \frac{1}{2}(u-d)^2$ (for simplicity, we omit the sampling operator at the receiver location hereinafter) is adopted in the FWI, where u and d are synthetic and observed seismograms. Its corresponding adjoint source is

$$\frac{\partial J_W}{\partial u} = u - d. \tag{7}$$

Besides, we introduce the traveltime and amplitude objective function (Tromp et al., 2005): $J_T = \frac{1}{2}\Delta T^2$ with $\Delta T = T_u - T_d$, where T_u and T_d are the traveltimes for synthetic and observed seismograms, respectively; $J_A = \frac{1}{2}\Delta A^2$ with $\Delta A = \frac{A_u - A_d}{A_d}$, where $A_u = \int_{t_1}^{t_2} u^2 dt$, $A_d = \int_{t_1}^{t_2} d^2 dt$ and (t_1, t_2) defines the time window to measure the misfit. Hence, their formulations of the adjoint sources can be derived using implicit differentiation technique (Luo and Schuster, 1991; Dahlen and Baig, 2002):

$$\frac{\partial J_T}{\partial u} = \Delta T \cdot \frac{\dot{u}}{\int_{t_1}^{t_2} u\ddot{u} dt}, \tag{8}$$

$$\frac{\partial J_A}{\partial u} = \Delta A \cdot \frac{u}{A_u A_d}. \tag{9}$$

Adjoint operator

In order to materialize Equation (5), we need to derive the explicit form of $\mathbf{L}^* = \mathbf{L_0^*} + \mathbf{L_1^*} + \mathbf{L_2^*}$. Recall $(\nabla^2)^* = \nabla^2$ and $(\frac{\partial}{\partial t})^* = -\frac{\partial}{\partial t}$, we can infer that the acoustic propagator is self-adjoint: $\mathbf{L_0^*} = \mathbf{L_0}$. In the following, we validate that the fractional Laplacian operators $(-\nabla^2)^{\frac{1}{2}}$ and $(-\nabla^2)^{\frac{3}{2}}$ are both self-adjoint by conducting dot product tests.

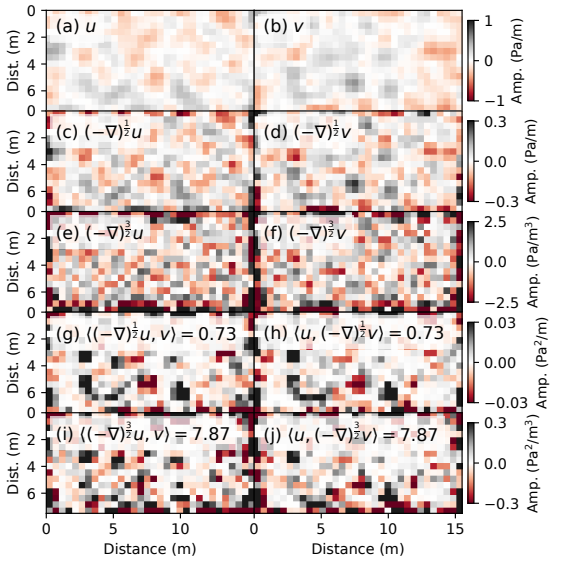

Figure 1: The dot product test of the fractional Laplacian operators for one random wavefield pair.

Since the fractional Laplacians are spatial derivative operators, we can consider the dot product in only one single time slice without the need for time integral. We generate two random wavefields (Figures 1a and 1b) and apply fractional Laplacians to them (Figures 1 c-f). Then we compute the element-by-element multiplication between Figures 1(c), 1(e) and Figures 1(d), 1(f), as shown in Figures 1(g)-(j). The summation of all the resultant elements for each figure yields the inner product and it appears that for these two random wavefields u and v, we have $\langle(-\nabla^2)^{\frac{1}{2}}u, v\rangle = \langle u, (-\nabla^2)^{\frac{1}{2}}v\rangle$ and $\langle(-\nabla^2)^{\frac{3}{2}}u, v\rangle = \langle u, (-\nabla^2)^{\frac{3}{2}}v\rangle$. Moreover, we conduct tests for another 100 random wavefield pairs and the fractional Laplacian operators pass the test for each pair. Thus, we can conclude that both $(-\nabla^2)^{\frac{1}{2}}$ and $(-\nabla^2)^{\frac{3}{2}}$ are self-adjoint.

Hence, we have $\mathbf{L_1^*} = \mathbf{L_1}$ and $\mathbf{L_2^*} = -\mathbf{L_2}$ so that $\mathbf{L}^* = \mathbf{L_0} + \mathbf{L_1} - \mathbf{L_2}$. Physically, it means that the adjoint operator of the viscoacoustic propagator compensates (anti-attenuates) the amplitude of the waves while preserves the velocity dispersion character (Zhu, 2014; Zhu et al., 2014). However, since we simulate the adjoint wavefield in a time reversal mode, the reversed adjoint wavefield attenuates rather than compensates the amplitude as the forward wavefield:

$$\mathbf{L}q^\ddagger = (\frac{\partial J}{\partial u})^\ddagger, \tag{10}$$

where $\ddagger$ indicates the time reversal.

Wavefield interaction

The last step to compute the Fréchet kernel is interacting the forward and adjoint wavefields, which requires an explicit formulation of equation (6). The Fréchet

kernel K can be separated into three parts as $\mathbf{L}$ does: $K = K_0 + K_1 + K_2$, where $K_i = -\langle q, \frac{\partial \mathbf{L_i}}{\partial m} u \rangle$ $(i = 0, 1, 2)$. In this study, we regard c and γ as the model parameters. Then the operators $\frac{\partial \mathbf{L_i}}{\partial m}$ can be derived directly from Equations (2)-(4). In particular, $\frac{\partial \mathbf{L_0}}{\partial c} = -\frac{2}{c^3}\frac{\partial^2}{\partial t^2}$, $\frac{\partial \mathbf{L_1}}{\partial c} = \frac{\gamma\omega_0}{c^2}(-\nabla^2)^{\frac{1}{2}} + \frac{\gamma}{\omega_0}(-\nabla^2)^{\frac{3}{2}}$, $\frac{\partial \mathbf{L_2}}{\partial c} = -\frac{\pi\gamma}{c^2}(-\nabla^2)^{\frac{1}{2}}\frac{\partial}{\partial t}$, $\frac{\partial \mathbf{L_0}}{\partial \gamma} = 0$, $\frac{\partial \mathbf{L_1}}{\partial \gamma} = -\frac{\omega_0}{c}(-\nabla^2)^{\frac{1}{2}} + \frac{c}{\omega_0}(-\nabla^2)^{\frac{3}{2}}$, and $\frac{\partial \mathbf{L_2}}{\partial \gamma} = (\frac{\pi}{c}(-\nabla^2)^{\frac{1}{2}} - \frac{2\pi\gamma}{\omega_0}\nabla^2)\frac{\partial}{\partial t}$.

NUMERICAL EXAMPLES

Kernel gallery

We implement the adjoint formulations derived in the previous section to compute the Fréchet kernels of a homogeneous model for the three different objective functions. To do that, we set up a 2-D target model on a 400 $\times$ 200 grid with spacing of 10 m in both directions. The target model has a reference phase velocity 3.05 km/s at 20 Hz with the quality factor $Q = 80$. We put a receiver at (3.7, 1) km and the source at (0.3, 1) km with a 20 Hz Ricker wavelet. We simulate the synthetic seismogram with 1 ms time interval as the ground truth data.

In the meantime, we set up an initial model on the same grid with 3 km/s reference phase velocity and $Q = 100$. First, we simulate the forward wavefield according to Equation (1). After that, the synthetic recorded at the receiver as well as the data is used to generate the adjoint source for different objective functions based on Equations (7)-(9). Next, we excite the adjoint source at the location of the receiver and simulate the adjoint wavefield in a reverse time order as Equation (10). Finally, the forward and adjoint wavefields are interacted to assemble the Fréchet kernels as Equation (6).

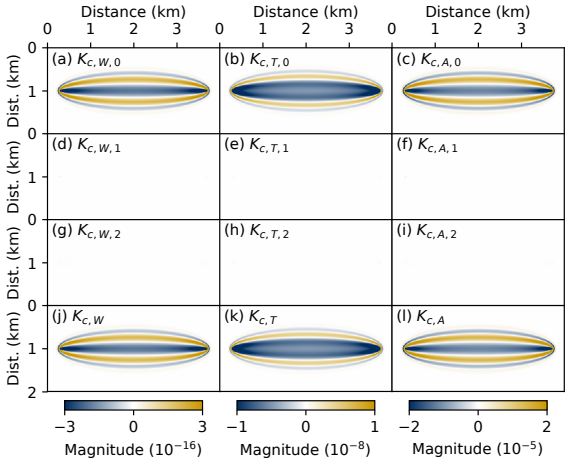

Figure 2: Velocity Fréchet kernels for waveform, traveltime and amplitude objective functions.

The first column of Figure 2 shows the velocity c kernel of different operator ($\mathbf{L_0}$, $\mathbf{L_1}$ and $\mathbf{L_2}$) contributions as well as their summation for the waveform objective function. The waveform kernels of attenuation γ are shown in the first column of Figure 3. Besides, the c and γ kernels for the traveltime and amplitude objective functions are shown in the rest of Figure 2 and 3, respectively. It appears that the c kernel is dominated by the contribution of acoustic propagator $\mathbf{L_0}$ compared to $\mathbf{L_1}$ and $\mathbf{L_2}$. On the contrary, γ has absolutely no sensitivity of $\mathbf{L_0}$ but is determined by the dispersion term $\mathbf{L_1}$ and the dissipation term $\mathbf{L_2}$. Moreover, the $\mathbf{L_2}$ contribution dominates the γ kernel for each of the objective functions, which is consistent with the fact that the amplitude loss is the first order viscoacoustic phenomenon compared to the velocity dispersion.

Furthermore, since the target model has higher c compared to the initial model, we would expect that the majority of the c kernel to be negative. In this sense, the traveltime kernel is more likely to benefit the convergence compared to the other two. On the other hand, the target model also has higher γ (lower Q) as both the waveform and the amplitude γ kernels capture this feature almost equally well. However, the traveltime γ kernel has a flipped polarity. Since the attenuation is barely sensitive to the traveltime phase shift, the traveltime γ kernel generally should not be used to update the model.

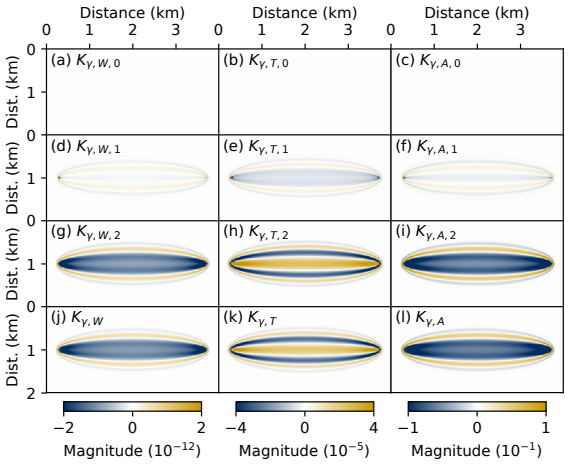

Figure 3: Attenuation Fréchet kernels for waveform, traveltime and amplitude objective functions.

Finite difference validation

To validate our algorithm, in this section, we use finite difference (FD) method to compute the kernels of a small (80 $\times$ 30) model and compare them with the ones obtained by the adjoint-state method. The adjoint kernels are computed as illustrated in the previous section. As for the FD kernels, we first compute the objective function, which is the misfit between the data and the synthetic generated by the initial model. For one single grid point of the initial model, we perturb the parameter (c or γ) by 10%, which leads to the model perturbation

10.1190/segam2019-3215198.1

Δm. We simulate the synthetic using this perturbed model and compute the new misfit, which has a subtle difference ΔJ compared to the original objective function. The Fréchet kernel value at this grid point is then assigned as $\frac{\Delta J}{\Delta m}$ and we iterate this process for all the grid points in the model. The comparison between the resultant kernels provided by two methods is shown in Figure 4. We only show the waveform and amplitude kernels since the tiny traveltime change caused by the perturbation of one grid point cannot be measured by the cross-correlation method, which results in zero traveltime FD kernels. It turns out that the kernels generated by both methods are consistent with each other thus it validates our adjoint-state algorithm.

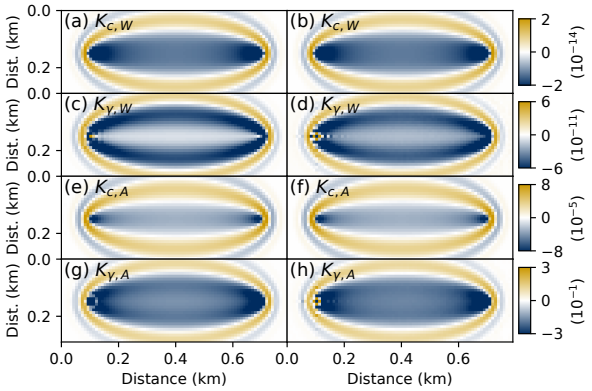

Figure 4: Adjoint (left) and FD (right) Fréchet kernels. The FD kernels are scaled appropriately to match the adjoint kernels.

Circular anomaly model

In this section, we demonstrate the capability of Fréchet kernels to characterize the velocity or attenuation anomaly. In this test, the initial model is the same homogeneous model as in the first numerical example. Compared to the initial model, the target model has a circular (radius 0.3 km) velocity anomaly of 3.1 km/s centered at (1.5, 0.8) km, which is smoothed by a Gaussian filter. We have 98 sources/receivers evenly distributed on the four margins of the model. The c and γ Fréchet kernels are computed for each shot and the stacked kernels are shown in Figure 5 for the three objective functions. Both the waveform and the traveltime c kernels reveal the velocity anomaly while the amplitude kernel has significant artifacts. Hence, the former two kernels should be utilized to invert for velocity. Meanwhile, the γ kernels indicate that there is a cross-talk between the velocity and attenuation.

The second test is conducted for a target model with a $Q = 50$ anomaly at the same position and the resultant kernels are shown in Figure 6. As expected, the waveform and the amplitude γ kernels delineate the anomaly while the traveltime has the least sensitivity to the Q variation. The leakage to the incorrect parameter (velocity) also exists in this test as shown by the c kernels.

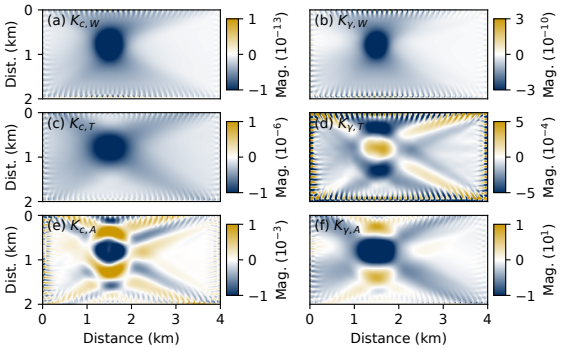

Figure 5: Fréchet kernels for the velocity anomaly.

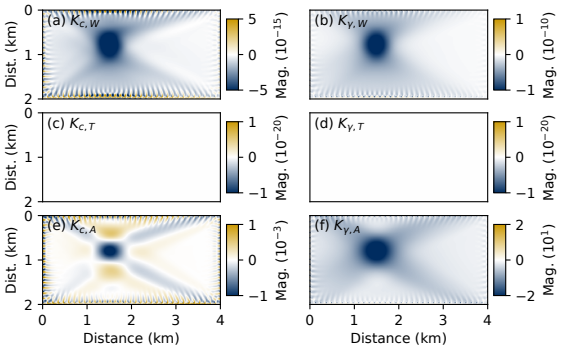

Figure 6: Fréchet kernels for the Q anomaly.

DISCUSSION AND CONCLUSIONS

We establish the formulations to compute the Fréchet kernels of the fractional viscoacoustic wave equation for different objective functions. In particular, we demonstrate that the adjoint modeling operator compensates the amplitude, though the adjoint wavefield is attenuating since it is simulated in a reverse time order. Also, according to the contribution from different operators ($\mathbf{L_0}$, $\mathbf{L_1}$ and $\mathbf{L_2}$), the acoustic propagator dominates the velocity kernel while the dissipation corrector dominates the attenuation kernel. Numerical examples suggest that it might be robust to first use traveltime and amplitude as objective functions to invert for velocity and attenuation, respectively; when the initial model is close enough to the target model, we might then adopt the waveform objective function to further refine the model. These Fréchet kernels lay the foundation of the waveform inversion and how to combine them to guarantee the convergence of the multiparameter inversion will be investigated in the future work.

ACKNOWLEDGMENTS

This work was supported by the National Energy Technology Laboratory of the U.S. Department of Energy, under the U.S. DOE Contract No. DE-FE0031544.

REFERENCES

Bai, J., D. Yingst, R. Bloor, and J. Leveille, 2014, Viscoacoustic waveform inversion of velocity structures in the time domain viscoacoustic waveform inversion: Geophysics, **79**, no. 3, R103–R119, doi: https://doi.org/10.1190/geo2013-0030.1.

Carcione, J. M., D. Kosloff, and R. Kosloff, 1988, Wave propagation simulation in a linear viscoelastic medium: Geophysical Journal International, **95**, 597–611, doi: https://doi.org/10.1111/j.1365-246X.1988.tb06706.x.

Chen, H., H. Zhou, Q. Li, and Y. Wang, 2016, Two efficient modeling schemes for fractional Laplacian viscoacoustic wave equation: Geophysics, **81**, no. 5, T233–T249, doi: https://doi.org/10.1190/geo2015-0660.1.

Dahlen, F., and A. M. Baig, 2002, Fréchet kernels for body-wave amplitudes: Geophysical Journal International, **150**, 440–466, doi: https://doi.org/10.1046/j.1365-246X.2002.01718.x.

Dvorkin, J. P., and G. Mavko, 2006, Modeling attenuation in reservoir and nonreservoir rock: The Leading Edge, **25**, 194–197, doi: https://doi.org/10.1190/1.2172312.

Emmerich, H., and M. Korn, 1987, Incorporation of attenuation into time-domain computations of seismic wave fields: Geophysics, **52**, 1252–1264, doi: https://doi.org/10.1190/1.1442386.

Fichtner, A., and M. van Driel, 2014, Models and Fréchet kernels for frequency-(in)dependent Q: Geophysical Journal International, **198**, 1878–1889, doi: https://doi.org/10.1093/gji/ggu228.

Kjartansson, E., 1979, Constant Q-wave propagation and attenuation: Journal of Geophysical Research: Solid Earth, **84**, 4737–4748, doi: https://doi.org/10.1029/JB084iB09p04737.

Knopoff, L., 1964, Q: Reviews of Geophysics, **2**, 625–660, doi: https://doi.org/10.1029/RG002i004p00625.

Luo, Y., and G. T. Schuster, 1991, Wave-equation traveltime inversion: Geophysics, **56**, 645–653, doi: https://doi.org/10.1190/1.1443081.

McDonal, F., F. Angona, R. Mills, R. Sengbush, R. Van Nostrand, and J. White, 1958, Attenuation of shear and compressional waves in Pierre shale: Geophysics, **23**, 421–439, doi: https://doi.org/10.1190/1.1438489.

Müller, T. M., B. Gurevich, and M. Lebedev, 2010, Seismic wave attenuation and dispersion resulting from wave- induced flow in porous rocks — A review: Geophysics, **75**, no. 5, 75A147–75A164, doi: https://doi.org/10.1190/1.3463417.

Plessix, R.-E., 2006, A review of the adjoint-state method for computing the gradient of a functional with geophysical applications: Geophysical Journal International, **167**, 495–503, doi: https://doi.org/10.1111/j.1365-246X.2006.02978.x.

Robertsson, J. O., J. O. Blanch, and W. W. Symes, 1994, Viscoelastic finite-difference modeling: Geophysics, **59**, 1444–1456, doi: https://doi.org/10.1190/1.1443701.

Tarantola, A., 1988, Theoretical background for the inversion of seismic waveforms, including elasticity and attenuation, *in* Scattering and Attenuations of Seismic Waves, Part I: Springer, 365–399, doi: https://doi.org/10.1007/978-3-0348-7722-0.

Tromp, J., C. Tape, and Q. Liu, 2005, Seismic tomography, adjoint methods, time reversal and banana-doughnut kernels: Geophysical Journal International, **160**, 195–216, doi: https://doi.org/10.1111/j.1365-246X.2004.02453.x.

Virieux, J., and S. Operto, 2009, An overview of full-waveform inversion in exploration geophysics: Geophysics, **74**, no. 6, WCC1–WCC26, doi: https://doi.org/10.1190/1.3238367.

Wang, N., H. Zhou, H. Chen, M. Xia, S. Wang, J. Fang, and P. Sun, 2017, A constant fractional-order viscoelastic wave equation and its numerical simulation scheme: Geophysics, **83**, no. 1, T39–T48, doi: https://doi.org/10.1190/geo2016-0609.1.

White, J., 1975, Computed seismic speeds and attenuation in rocks with partial gas saturation: Geophysics, **40**, 224–232 doi: https://doi.org/10.1190/1.1440520.

Xing, G., and T. Zhu, 2018, Fractal mechanical network based time domain viscoacoustic wave equation: 88th Annual International Meeting, SEG, Expanded Abstracts, 3994–3998, doi: https://doi.org/10.1190/segam2018-2995782.1.

Xue, Z., J. Sun, S. Fomel, and T. Zhu, 2017, Accelerating full-waveform inversion with attenuation compensation: Geophysics, **83**, no. 1, A13–A20, doi: https://doi.org/10.1190/geo2017-0469.1.

Yang, J., and H. Zhu, 2018, A time-domain complex-valued wave equation for modelling visco-acoustic wave propagation: Geophysical Journal International, **215**, 1064–1079, doi: https://doi.org/10.1093/gji/ggy323.

Yang, P., R. Brossier, L. Métivier, and J. Virieux, 2016, A review on the systematic formulation of 3-D multiparameter full waveform inversion in viscoelastic medium: Geophysical Journal International, **207**, 129–149, doi: https://doi.org/10.1093/gji/ggw262.

Zhu, T., 2014, Time-reverse modelling of acoustic wave propagation in attenuating media: Geophysical Journal International, **197**, 483–494, doi: https://doi.org/10.1093/gji/ggt519.

Zhu, T., and J. M. Carcione, 2013, Theory and modelling of constant-Q P-and S-waves using fractional spatial derivatives: Geophysical Journal International, **196**, 1787–1795, doi: https://doi.org/10.1093/gji/ggt483.

Zhu, T., and J. M. Harris, 2014, Modeling acoustic wave propagation in heterogeneous attenuating media using decoupled fractional Laplacians: Geophysics, **79**, no. 3, T105–T116, doi: https://doi.org/10.1190/geo2013-0245.1.

Zhu, T., J. M. Harris, and B. Biondi, 2014, Q-compensated reverse-time migration: Geophysics, **79**, no. 3, S77–S87, doi: https://doi.org/10.1190/geo2013-0344.1.